

## Design of a Bézier-Profile Horn for High Displacement Amplification

D.-A. Wang<sup>a,\*</sup>, W.-Y. Chuang<sup>b</sup>, K. Hsu<sup>b</sup>, H.-T. Pham<sup>a</sup>

<sup>a</sup>*Institute of Precision Engineering, National Chung Hsing University, Taichung 402, Taiwan, ROC*

<sup>b</sup>*Precision Machinery Research and Development Center, Taichung 407, Taiwan, ROC*

June 10, 2010

### Abstract

A new horn for high displacement amplification is developed. The profile of the horn is a cubic Bézier curve. The ultrasonic actuation of the horn exploits the first longitudinal displacement mode of the horn. A design method of the horn using an optimization scheme and finite element analyses is developed. Prototypes of the horns are manufactured by a numerical control machining process. Performances of the proposed horn have been evaluated by experiments. Experimental results of the harmonic response of the fabricated horn confirm the effectiveness of the design method. The displacement amplification of the proposed horn is 71% higher than that of the traditional catenoidal horn with the same length and end surface diameters.

*PACS:* 87.55.de; 06.30.Bp

*Keywords:* Bézier horn; Optimization; Ultrasonic actuation; Displacement amplification

---

\* Corresponding author. Tel.:+886-4-22840531; fax:+886-4-22858362

*E-mail address:* daw@dragon.nchu.edu.tw (D.-A. Wang).

## 1. Introduction

Use of improved high displacement ultrasonic horns for various applications of atomizers [1], ophthalmic surgery [2], welding devices [3], wire bonding [4,5], ultrasonic motor [6], ultrasonic lubrication [7] and ultrasonic bistoury [8] etc. continues to be a field of interest. Ultrasonic horns of different profiles such as Gaussian [9], Fourier, exponential [10], stepped [11,12], sinusoidal [13], conical, catenoidal [14], have been proposed and investigated by many researchers. Salmon [15] synthesized a horn where the profile is a perturbation from the exponential contour. In comparing with the traditional horns, new horns with non-straight structures may offer higher displacement amplification. Sherrit et al. [16] presented a folded horn in order to reduce the length of the resonator. Iula et al. [17] proposed an ultrasonic horn vibrating in a flexural mode. Its displacement amplification is about 50% higher than that of the stepped horn.

The most commonly used horns are conical, exponential, catenoidal, stepped and Gaussian [18]. Abromov [18] points out that the displacement amplification of catenoidal horns is greater than that of exponential or conical ones and less than that of stepped horns. Gaussian horns may possess high displacement amplification. However, numerical methods might be needed for design of Gaussian horns. Table 1 lists the positive and negative aspects of several commonly used horn profiles. Development of new horns is needed in applications where very high displacement amplification and simple transducer structure are required.

Parametric curves may be used to describe the profiles of horns for high displacement amplification and ease of machining. In parametric form each coordinate of a point on a curve is represented as a function of a single parameter [19]. Parametric

curve based geometry is flexible enough to give a much better control over the profile of horns for design purpose. Therefore, it has more potential to find higher displacement amplification while keeping the stress in the horns low. Because the parametric curve has more freedom to define the horn profile, it is a more difficult problem to optimize the performance of the horn. Finite element method (FEM) has been used to study and analyze behaviors of horns [17,20]. Using FEM, detailed stress and displacement distributions can be obtained. Fu et al. [21] discussed the design of a piezoelectric transducer with a stepped horn via multiobjective optimization. They formulated the optimization problem using Pareto-based multiobjective genetic algorithms [21]. In order to design horns with conflicting design objectives, the genetic algorithms capable of finding multiple optimal solutions in a single optimization run may be used.

In this paper, we develop a new horn for high displacement amplification. The design is based on a cubic Bézier curve. The optimal designs of the horns are sought by a multiobjective optimization algorithm. Three-dimensional finite element analyses are carried out to evaluate the mechanical behaviors of the horns. Prototypes of horns are fabricated by a numerical control (NC) machining process. Displacements and resonant frequencies of the horns are obtained by a fiber optic displacement sensor. The experimental results are compared with the optimized solutions and the results of finite element analyses.

## **2. Horn design**

Fig. 1 schematically shows a horn driven by a Langevin transducer. A Cartesian coordinate system is also shown in the figure. The horn is a displacement amplifier

designed to work in its first longitudinal mode. The Langevin transducer is composed of a couple of piezoelectric disks poled along  $y$  direction but with opposite polarities and two aluminum cylinders, front and back metal blocks, which have radius identical to that of the disks. The flange allows the mounting of the Langevin transducer at the longitudinal nodes. The horn is actuated by the transducer at the designated frequency, which is set to be the working frequency, 27.9 kHz, of the Langevin transducer used in the experiments. The nearly uniformly distributed displacement of the Langevin transducer is transformed into a longitudinal deformation of the horn. A typical displacement distribution curve is also shown in the figure. By proper design of the horn structure, the longitudinal mode of vibration of the horn can be excited, and a large displacement amplification can be obtained.

The design of the horn for high displacement magnification is based on an optimization procedure where the profile of the horn is optimized via the parameters of a cubic Bézier curve to meet the requirement of displacement amplification. The cubic Bézier curve is determined by a four-point Bézier polygon  $Q_0Q_1Q_2Q_3$  as shown in Fig. 2. As described by Rogers and Adams [19], the first and last points,  $Q_0$  and  $Q_3$ , respectively, on the curve are coincident with the first and last points of the defining polygon. The tangent vectors at the ends of the curve have the same directions as the first and last polygon spans, respectively. The parametric cubic Bézier curve is given by [19]

$$P(t) = \begin{bmatrix} (1-t)^3 & 3t(1-t)^2 & 3t^2(1-t) & t^3 \end{bmatrix} \begin{bmatrix} P_{Q_0} \\ P_{Q_1} \\ P_{Q_2} \\ P_{Q_3} \end{bmatrix} \quad 0 \leq t \leq 1 \quad (1)$$

where  $t$  is the parameter, and  $P_{Q_i}$  is the position vector of the point  $Q_i$ .

The profile of the horn is optimized by allowing points  $Q_1$  and  $Q_2$  to move in the design space enclosed by the dashed rectangle in Fig. 2. The positions of the points  $Q_0$  and  $Q_3$  are fixed by the specified radius of the back and front end of the horn,  $R_1$  and  $R_2$ , respectively, and the length of the horn,  $L$ . The horn is assumed to be axisymmetric. An optimization procedure is developed and outlined in Fig. 3. The nondominated sorting genetic algorithm [22] is applied to the optimization of the horn profile. The algorithm is suitable for solving constrained multiobjective problems. In the evolution process of the genetic algorithm, the following are performed in each generation.

- Select the parents which are fit for reproduction: Parents are selected for reproduction to generate offspring. The genetic algorithm uses a binary tournament selection and the crowded-comparison operator [22]. In the binary tournament selection process, two individuals are selected at random and their fitness is compared. The individual with better fitness is selected as a parent. The crowded-comparison operator guides the selection process at the various stages of the algorithm toward a uniformly spread-out Pareto-optimal front [22].
- Perform crossover and mutation operator on the selected parents: The algorithm uses simulated binary crossover and polynomial mutation [22].
- Perform Selection from the parents and the offspring: Once the population is sorted based on the nondominated sorting algorithm, only the best solutions are selected.
- Replace the unfit individuals with the fit individuals to maintain a constant population size.

In the optimization process as shown in Fig. 3, initially, the working frequency  $f$  and the geometry parameters  $R_1$ ,  $R_2$  and  $L$  are specified. The objective functions of the optimization problem are

$$\begin{aligned} \text{Min} \quad & f - f_0 \\ \text{Max} \quad & M = \frac{u_{Q_3}}{u_{Q_0}} \end{aligned} \quad (2)$$

where  $f_0$  is the first longitudinal modal frequency of the population of each generation of the horn.  $M$  is the amplification of the displacement defined by the ratio of the longitudinal displacement at the front end to that of the back end of the horn. The fast nondominated sorting approach [22] is used to solve the two-objective optimization problem. In the sorting procedure, the concept of Pareto dominance [23] is utilized to evaluate fitness or assigning selection probability to solutions. The population is classified into non-dominated fronts based on its rank in the population, not its actual objective function values.

The proposed horn is designed to have the same working frequency as the Langevin transducer. Due to the geometry complexity, the modal frequency  $f_0$  and the displacement amplification  $M$  of the Bézier horn cannot be calculated analytically. Finite element analysis by a commercial software ANSYS is utilized to obtain  $f_0$  and  $M$  of the horn. The genetic algorithm optimization procedure used in this investigation is programmed with the commercial software MATLAB 7.0. The genetic algorithm, the design parameters (the 4 control points  $Q_i$  of the Bézier curve) and the geometry constraints are written in a script file of MATLAB. The profile of the horn is calculated and the coordinates of all nodes along the profile is created in the script file. An ANSYS

text file for the harmonic analysis to obtain the modal frequency  $f_0$  and the displacement amplification  $M$  is created by the MATLAB file. The output of the ANSYS harmonic simulation is saved in a text file. The first longitudinal modal frequency and the displacement distribution along the horn can be found in the file, and are used as the objective functions for the optimization process.

### 3. Analyses

#### 3.1 Finite element model

In order to obtain accurate modal frequency and displacement solutions for the proposed horn, finite element analyses are carried out. Fig. 4(a) shows a schematic of a Langevin transducer and a Bézier horn. The horn has a length  $L$  and diameters  $D_1$  and  $D_2$  of its back and front ends, respectively. The dimensions of the Langevin transducer are indicated in the figure. A Cartesian coordinate system is also shown in the figure. Fig. 4(b) shows a mesh for a three-dimensional finite element model. The finite element model has 46116 8-node elements. A mesh convergence study is performed to obtain accurate solutions of displacement solutions. The displacements in the  $x$  and  $z$  directions of the nodes on the circumference of the nodal flange are constrained. A voltage is applied to the piezoelectric disk for harmonic analyses of the Langevin transducer and the horn.

In this investigation, the piezoelectric disk, front and back metal blocks of the Langevin transducer, and the horn are assumed to be linear elastic materials. A lead zirconate titanate material (PZT-5H), an aluminum alloy (AA 7075), and mild steel (SS 41) are used for the piezoelectric disk, the metal blocks of the Langevin transducer, and

the horn material, respectively. Their material properties are listed in Table 2. The commercial finite element program ANSYS is employed to perform the computations. 8-node quadratic element Solid185 is used for the finite element model, except that 8-node quadratic element Solid5 is used to model the piezoelectric disk.

### 3.2 Numerical analysis

In the optimization process, the number of generations,  $N$ , is set to be 40, and the population of each generation is taken as 20. In the analyses, we have also set  $N = 50, 60, 70, 80, 90$  and  $100$ . However, there is no improvement with  $N$  greater than 40. The length  $L$  and the diameters  $D_1$  and  $D_2$  of the back and front end of the horn are specified as 93 mm, 20 mm and 5 mm, respectively. The working frequency  $f$  is set to be 27.9 kHz. In the experiments, the fabricated horn is driven by a Langevin transducer. The available commercial Langevin transducer is purchased from a local vendor. The working frequency of the Langevin transducer is a known and fixed parameter.

A modal analysis of each population is performed in order to find its first longitudinal modal frequency  $f_0$  and displacement amplification  $M$ . A typical normalized frequency response function (FRF) of the model including the Langevin transducer and the horn during the optimization process is shown in Fig. 5. The figure shows that two modes are responsive when the system is excited longitudinally in a frequency range of 0-50 kHz, based on the finite element analyses. Both modes with the modal frequencies of 27.9 and 41.0 kHz, respectively, are longitudinal. It is recognized that the operational mode at 27.9 kHz shown in the normalized FRF is significantly overshadowed by the second order longitudinal mode at 41.0 kHz. Based on the finite

element analyses, both the transducer and the horn vibrate longitudinally at 27.9 kHz and 41.0 kHz and the response level of the transducer alone excited at 41.0 kHz is much larger than that excited at 27.9 kHz. Clearly if the system is excited at or very close to 27.9 kHz, then there should be no modal coupling to 41.0 kHz. The results shown in this figure suggest that the assembly should be operating at 41.0 kHz. Since the working frequency of the Langevin transducer available is fixed at 27.9 kHz, the Bézier horn is designed to have its first longitudinal modal frequency equal to the working frequency of the transducer in this investigation.

A large number of modes should be responsive when the horn is excited longitudinally in the frequency range of 0-50 kHz, but Fig. 5 only illustrates two longitudinal modes since the responses of many modes are small compared to the two longitudinal modes. In order to characterize the intermodal responses, the mode combinations for possible combination resonance are considered. Three of the mode shapes are shown in Fig. 6. The whole system modes involve contributions from the horn and the transducer. These modes, corresponding to a bending mode of the assembly (Fig. 6(a)), a horn radial expansion and transducer torsion mode (Fig. 6(b)), and a longitudinal mode of the assembly (Fig. 6(c)), occur at 7991 Hz ( $\omega_2$ ), 19993 Hz ( $\omega_3$ ) and 27823 Hz ( $\omega_1$ ), respectively, and satisfy the combination resonance,  $\omega_1 \cong \omega_2 + \omega_3$ . When the system is excited close to its first longitudinal mode, the internal modes, excited through the combination resonance, are excited at a much smaller response levels as seen in Fig. 5. It is assumed that modal interactions may not occur. This assumption is verified by the experimental measurements of the flexural displacement of the horn when the horn is driven longitudinally in the frequency range of 0-50 kHz.

Fig. 7 shows the distribution of the population of several generations in the optimization process. The abscissa represents the difference between  $f$  and  $f_0$ . The ordinate represents the displacement amplification. The displacement amplification is determined by the ratio of the front-end displacement to the back-end displacement of the horn. The displacement amplification is increased dramatically after 40 generations. As also shown in the figure, the difference between  $f$  and  $f_0$  of the best of the population in each generation is nearly zero. Fig. 8 shows the profile of an optimized Bézier horn. The position of its control points are also shown in the figure.

In order to compare the performances of the proposed horn with classical horns, a catenoidal horn and a stepped horn are also modeled. As listed in Table 1, the stepped horn has the largest displacement amplification among the commonly used horns. However, its high stress occurring near the abruptly changing section is not favored. The catenoidal horn has smaller displacement amplification and a smoother stress distribution than the stepped horn. The new horn discussed in this paper may have larger displacement amplification than the catenoidal horn, and lower stress concentration than the stepped horn. Here, the stepped, catenoidal and Bézier horns are selected based on the criteria of displacement amplification and Mises stress.

For fair comparison, the catenoidal horn has the same back and front end radiuses and length as those of the proposed horn. The working frequency of the catenoidal horn obtained by a finite element analysis is 28.3 kHz. The back and front end radiuses of the stepped horn are the same as those of the proposed horn. In order to have the same working frequency of 27.9 kHz as the proposed horn, the length of the stepped horn can be calculated analytically by assuming the length of both sections equal to a quarter of

the ultrasonic wavelength of the material. The calculated length of the stepped horn is 91 mm. The profiles of the catenoidal and stepped horns are also shown in Fig. 8.

Fig. 9 is a plot of the normalized displacements along the normalized length of the horns based on finite element computations. The displacements are normalized by the displacement at the back end of the horns. Therefore, the normalized displacement at the normalized length of 1 represents the displacement amplification. The stepped horn has the largest displacement amplification among the three types of the horns. The displacement amplification of the Bézier horn is nearly twice of that of the catenoidal horn. Fig. 10 shows the von Mises stress along the normalized length of the horns based on the finite element computations. For the stepped horn, high stress occurs near the abruptly changing section. Stress concentration of the Bézier horn is significantly less than the other two types of horns. The lower Von Mises stress of the proposed horn can be attributed to its bell-shaped profile. The values of the displacement amplification  $M$  and maximum von Mises stress  $\sigma_{\max}$  of the three types of the horns are listed in Table 3. Although the stepped horn gives the highest displacement amplification, its high stress concentration at the step discontinuity makes it prone to failure.

#### **4. Fabrication, experiments and discussions**

In order to verify the effectiveness of the proposed horn, prototypes of a Bézier horn and a catenoidal horn are fabricated by a numerical control machining from a stainless steel. Dimensions of the prototypes are based on the finite element analyses. Fig. 11 is a photo of the fabricated horns. The horns are driven by the Langevin transducer. Fig. 12(a) is a schematic of the experimental apparatus for measurement of

the displacement/vibration of the horns driven in the longitudinal mode. The horns are mounted on an optical table. AC voltages are applied to the Langevin transducer by an electronic circuit that works like a nearly ideal voltage source. The vibration amplitude of the horns is measured by a fiber optic displacement/vibration sensor (MTI-2000, MTI Instruments Inc., US). The sensor probe is held by a micro manipulator. The measurement is recorded and analyzed by a data acquisition unit (PCI-5114, National Instruments Co., US).

In order to obtain the electrical power absorbed by the horns, a LCR meter (WK-4235, Wayne Kerr Electronics Ltd., UK) is used to measure the electrical input impedance of the horns. The test voltage of the LCR meter used in the experiments is  $2 V_{\text{rms}}$ . Fig. 13(a) and (b) show the electrical input impedance and phase, respectively, of the Bézier and the catenoidal horn. As shown in Fig. 13(a), the measured working frequency  $f_s^B$  of the Bézier horn is 27.9 kHz which is in a quite good agreement with that predicted in the analyses (see Fig. 5). For the catenoidal horn, the measured working frequency  $f_s^C$ , 28.3 kHz, is nearly the same as that obtained by the finite element analysis. The experimental results indicate that the modulus of the impedance of the proposed horn is lower than that of the catenoidal horn at their respective working frequencies. Since the two horns are tested with the same voltage; being the electrical impedance at the working frequency of the proposed horn lower than that at the working frequency of the catenoidal horn, the Bézier horn is able to absorb a higher electrical power than the catenoidal horn.

When the system is driven in the operating mode and a combination resonance occurs, then a large amount of energy flows from the operating mode to the internal

modes [24]. In the experiments, the system is excited close to its first longitudinal mode. It is assumed that the internal modes are not excited based on the finite element analyses. In order to verify this assumption, experiments are carried out to measure the flexural displacement/vibration of the horns driven in the longitudinal mode. Figs. 12(b) and (c) are photos of the experimental setup for measurement of the longitudinal and flexural displacements, respectively, of the horns driven in the longitudinal mode. The modal interactions should be investigated by using a 3D laser Doppler vibrometer. Due to the measurement equipments available, the fiber optic displacement/vibration sensor is used for initial assessment of the modal interactions. Figs. 14(a) and (b) show the measured longitudinal and flexural vibration amplitude, respectively, of the horn tip when the horn is driven longitudinally at 27.9 kHz. The responses of the longitudinal and flexural vibrations exhibited a single frequency response as shown in the figure. Some measurement noise of the flexural vibrations is also shown in Fig. 14(b). The noise can be attributed to the curved profile of the horn and the misalignment of the horn and the probe tip of the flexural vibration measurement setup.

Fig. 15 shows the measured vibration amplitude of the Bézier horn and the catenoidal horn as functions of the applied voltage at 27.9 kHz and 28.3 kHz, respectively. Three measurements are taken for each driving voltage. The variations of the measurements are indicated by the error bars in the figure. The vibration amplitudes of both horns increase as the driving voltage increases. The average displacement of the Bézier horn is approximately 50% greater than that of the catenoidal horn for the driving voltages considered. The displacement amplifications of the fabricated Bézier horn and the catenoidal horn driven at their first longitudinal modal frequency are 8.2 and 4.8,

respectively. The simulation results listed in Table 3 shows that the Bézier horn has the displacement amplification 78% larger than the catenoidal horn while the experiment shows a nearly 71% of improvement. The manufacturing error and the misalignment due to assembly process may contribute to the discrepancy. It should be noted that high power ultrasonic components are prone to non-linear response with cubic softening or hardening. The discrepancy may also be attributed to the assumption that the finite element analyses carried out in this investigation are based on linear dynamic response.

Fig. 16 is the harmonic response of the designed and fabricated Bézier horns near the working frequency, 27.9 kHz. The experimental working frequency of the Bézier horn, 27.9 kHz, is in a good agreement with that predicted by the finite element analyses without damping. When damping is considered in the finite element analysis, the simulated modal frequency should be lower than that without damping. It is suggested that the effects of damping on the first longitudinal modal frequency of the finite element model can be neglected due to the close agreement between the experiments and simulations for the purpose of the optimization design process of the proposed horn.

In this investigation, a cubic Bézier curve is chosen for the horn profile. When a Bézier polygon formed by connecting the control points is a convex hull, the Bézier curve must be contained in the polygon. However, in situations where Bézier polygons don't form a convex hull, Bézier curves may have cusps or loops. The cusp and loop may cause stress concentration and redundant segments for structure contours formed by Bézier curves. A cusp and loop avoiding algorithm for the cubic Bézier curve is developed in our shape optimization process. Higher orders of the Bézier curve usually have these two defects which lengthen the simulation time or cause unexpected

interruption in the optimization process. Therefore, a cubic Bézier curve is selected for the shape optimization of the proposed horn.

## **5. Conclusions**

A new horn with high displacement amplification is proposed. The profile of the horn is a cubic Bézier curve. A design procedure using a multiobjective optimization algorithm and finite element analyses is developed to optimize displacement amplification of the horn. This procedure can be used to design the horn with different displacement amplification and dimensional requirements. Prototypes of the horn have been fabricated and tested to verify the developed design method. The experimental results are in good agreement with the design specifications. The displacement amplification of the proposed horn is 71% higher than that of the traditional catenoidal horn with the same length and end surface diameters due to its capacity to absorb higher electrical power. Based on the finite element analyses, maximum von Mises stress of the proposed horn is much lower than that of the catenoidal horn. Furthermore, by driving the catenoidal and the Bézier horns at their respective working frequencies with the same voltage amplitude; it was verified that the Bézier horn is able to absorb a higher electrical power than the catenoidal horn.

Experimental comparison of the working frequency between the designed and fabricated Bézier horns validates the effectiveness of the optimization design method, even if the maximum displacement amplification of the fabricated horn is slightly lower than that predicted by simulations of the designed horn, due to the imperfection from the machining process. The proposed horn may be more suitable than the classical stepped

and catenoidal horns in application where high displacement amplification and low stress concentration are required.

### **Acknowledgement**

This work was financially supported by Precision Machinery Research and Development Center (Contract Number: 98TR10). Partial support of this work by a grant from National Science Council, Taiwan (Grant Number: NSC 96-2221-E-005-095) is greatly appreciated. The authors would like to express their appreciation to the National Center for High-Performance Computing (NCHC), Taiwan for their assistance. Helpful discussions with Mr. Yao-Tang Lin of Precision Machinery Research and Development Center are greatly appreciated.

## References

- [1] R. R. Perron, The design and application of a reliable ultrasonic atomizer, *IEEE Transactions on Sonics and Ultrasonics*, SU-14 (1967) 149-153.
- [2] S. Charles, R. Williams and T. L. Poteat, Micromachined structures in ophthalmic microsurgery, *Sensors and Actuators*, A21–A23 (1990) 263-266.
- [3] L. Parrini, Design of advanced ultrasonic transducers for welding devices, *IEEE Transactions on Ultrasonics, Ferroelectrics and Frequency Control*, 48 (2001) 1632-1639.
- [4] S. W. Or, H. L. W. Chan, V. C. Lo and C. W. Yuen, Dynamics of an ultrasonic transducer used for wire bonding, *IEEE Transactions on Ultrasonics, Ferroelectrics and Frequency Control*, 45 (1998) 1453-1460.
- [5] L. Parrini, New technology for the design of advanced ultrasonic transducers for high-power applications, *Ultrasonics*, 41 (2003) 261-269.
- [6] J. Hu, K. Nakamura and S. Ueha, An analysis of a noncontact ultrasonic motor with an ultrasonically levitated rotor, *Ultrasonics*, 35 (1997) 459-467.
- [7] A. Iula, G. Caliano, A. Caronti and M. Pappalardo, A power transducer system for the ultrasonic lubrication of the continuous steel casting, *IEEE Transactions on Evolutionary Computation*, 50 (2003) 1501-1508.
- [8] A. Iula, S. Pallini, F. Fabrizi, R. Carotenuto, N. Lamberti and M. Pappalardo, A high frequency ultrasonic bistoury designed to reduce friction trauma in cystectomy operations, in: Proceedings of 2001 IEEE Ultrasonics Symposium, 2001, pp. 1331-1334.
- [9] C.-H. Lee and A. Lal, Silicon ultrasonic horns for thin film accelerated stress testing, in: Proceedings of 2001 IEEE Ultrasonics Symposium, 2001, pp. 867-870.
- [10] E. Eisner, Design of sonic amplitude transformers for high magnification, *The Journal of the Acoustical Society of America*, 35 (1963) 1367-1377.
- [11] A. Bangviwat, H. K. Ponnekanti and R. D. Finch, Optimizing the performance of piezoelectric drivers that use stepped horns, *The Journal of the Acoustical Society of America*, 90 (1991) 1223-1229.
- [12] D. Sindayihebura and L. Bolle, Theoretical and experimental study of transducers aimed at low-frequency ultrasonic atomization of liquids, *The Journal of the*

*Acoustical Society of America*, 103 (1998) 1442-1448.

- [13] B. N. Nagarkar and R. D. Finch, Sinusoidal horns, *The Journal of the Acoustical Society of America*, 50 (1971) 23-31.
- [14] K. F. Graff, *Wave motion in elastic solids*, Oxford : The Clarendon Press, 1975.
- [15] V. Salmon, A new family of horns, *The Journal of the Acoustical Society of America*, 17 (1946) 212-218.
- [16] S. Sherrit, S. A. Askins, M. Gradziol, B. P. Dolgin, X. Bao, Z. Chang and Y. Bar-Cohen, Novel horn designs for ultrasonic/sonic cleaning welding, soldering, cutting and drilling, in: Proceedings of the SPIE Smart Structures Conference 2002, Vol. 4701, Paper No. 34, San Diego, CA.
- [17] A. Iula, L. Parenti, F. Fabrizi and M. Pappalardo, A high displacement ultrasonic actuator based on a flexural mechanical amplifier, *Sensors and Actuators A*, 125 (2006) 118-123.
- [18] O. V. Abramov, *High-intensity ultrasonics : theory and industrial applications*, Gordon and Breach Science Publishers, The Netherlands, 1998.
- [19] D. F. Rogers and J. A. Adams, *Mathematical elements for computer graphics*, 2<sup>nd</sup> edition, McGRAW-Hill, New York, 1990.
- [20] J. Woo, Y. Roh, K. Kang and S. Lee, Design and construction of an acoustic horn for high power ultrasonic transducers, in: Proceedings of 2006 IEEE Ultrasonics Symposium, 2006, pp. 1922-1925.
- [21] B. Fu, T. Hemsel and J. Wallaschek, Piezoelectric transducer design via multiobjective optimization, *Ultrasonics*, 44 (2006), e747-e752.
- [22] K. Deb, A. Pratap, S. Agarwal and T. Meyarivan, A fast and elitist multiobjective genetic algorithm: NSGA-II, *IEEE Transactions on Evolutionary Computation*, 6 (2002) 182-197.
- [23] D. E. Goldberg, *Genetic algorithms in search, optimization & machine learning*, Addison Wesley Publishing Company, Inc., MA, 1989.
- [24] A. Cardoni, M. Lucas, M. Cartmell and F. Lim, A novel multiple blade ultrasonic cutting device, *Ultrasonics*, 42 (2004), 69-74.

## **Biography**

**Dung-An Wang** received the Ph.D. degree in mechanical engineering from the University of Michigan at Ann Arbor, in 2004. He is currently an Assistant Professor in the Institute of Precision Engineering, National Chung Hsing University, Taiwan, ROC. His research interests include micromachined resonators and actuators, piezoelectric actuators, microassembly and compliant mechanisms.

**Wei-Yen Chuang** received the B.S. degree in mechanical engineering from the I-Shou University, Taiwan, ROC., in 2001, and the M.S degree in mechanical engineering from the National Yunlin University of Science and Technology, Taiwan, ROC., in 2003. He is currently an engineer in the Nano Technology Department, Precision Machinery Research and Development Center, Taiwan, ROC.

**Kei Hsu** received the B.S. degree in electrical engineering from the I-Shou University, Taiwan, in 1996, and the M.S degree in mechanical engineering in Chung Hua University, Taiwan, ROC., in 1998. He is currently the manager of the Nano Technology Department, Precision Machinery Research and Development Center, Taiwan, ROC.

**Huy-Tuan Pham** received the B.S. degree in mechanical engineering from the Ho Chi Minh City University of Technique, Vietnam, in 2005, and the M.S degree from the Institute of Precision Engineering, National Chung Hsing University, Taiwan, ROC., in 2008. He is currently working towards the Ph.D. degree in the Institute of Precision Engineering, National Chung Hsing University, Taiwan, ROC. His research interests are micromachined resonators and actuators, and compliant mechanisms.

Table 1. Positive and negative aspects of several commonly used horn profiles

Horn profile	Positive	Negative
Conical	Simple, easy to design and fabricate.	Lowest displacement amplification
Exponential	Smooth stress distribution	Low displacement amplification
Catenoidal	Displacement amplification greater than exponential, smooth stress distribution	Moderate displacement amplification
Bézier	Higher displacement amplification, lower stress concentration, applicable for non-straight horns (bend horns, asymmetric horns)	Design by numerical methods.
Stepped	Highest displacement amplification	High stress concentration, prone to break at the abrupt change of the profile.
Gaussian	May have large displacement amplification and low stress concentration.	Design by numerical methods.

Table 2. Properties of the piezoelectric disk (PZT-5H), metal blocks of the Langevin transducer (AA 7075) and the horn (SS 41)

Property		Tensor (in order of $x, y, z, xy, xz, yz$ )
PZT-5H	Piezoelectricity ( $\text{C m}^{-2}$ )	$\begin{bmatrix} 0 & -6.55 & 0 \\ 0 & 23.3 & 0 \\ 0 & -6.55 & 0 \\ 17.0 & 0 & 0 \\ 0 & 0 & 0 \\ 0 & 0 & 17.0 \end{bmatrix}$
	Permittivity ( $\text{F m}^{-1}$ )	$10^{-9} \times \begin{bmatrix} 15.052 & 0 & 0 \\ 0 & 13.015 & 0 \\ 0 & 0 & 15.052 \end{bmatrix}$
	Stiffness ( $\text{N m}^{-2}$ )	$10^{10} \times \begin{bmatrix} 12.72 & 8.47 & 8.02 & 0 & 0 & 0 \\ & 11.74 & 8.47 & 0 & 0 & 0 \\ & & 12.72 & 0 & 0 & 0 \\ & & & 2.30 & 0 & 0 \\ & \text{symmetric} & & & 2.35 & 0 \\ & & & & & 2.30 \end{bmatrix}$
	Density ( $\text{kg m}^{-3}$ )	7600
AA 7075	Young's modulus (GPa)	69
	Poisson's ratio	0.35
	Density ( $\text{kg m}^{-3}$ )	2730
SS 41	Young's modulus (GPa)	210
	Poisson's ratio	0.3
	Density ( $\text{kg m}^{-3}$ )	7800

Table 3. Comparison of the three types of the horns

	$R_1 / R_2$	Length (mm)	$M$	$\sigma_{\max}$ (MPa)
Catenoidal	4	93	5.9	76.5
Stepped	4	91	15.7	497
Bézier	4	93	10.5	32.4

### List of figures

- Fig. 1 Schematic of a horn and a Langevin transducer.
- Fig. 2 A profile of a Bézier horn and its four control points  $Q_0$ ,  $Q_1$ ,  $Q_2$  and  $Q_3$ .
- Fig. 3 Flowchart of the optimization procedure.
- Fig. 4. (a) Schematic of a horn and a Langevin transducer. (b) A mesh for a three-dimensional finite element model.
- Fig. 5. A typical normalized frequency response function of the model.
- Fig. 6. The internal modes determined by finite element analyses.
- Fig. 7. Distribution of the population of several generations in the optimization process.
- Fig. 8. Profiles of the horns.
- Fig. 9. Normalized displacements along the normalized length of the horns.
- Fig. 10. Von Mises stress along the normalized length of the horns.
- Fig. 11. Fabricated prototypes and a Langevin transducer.
- Fig. 12. (a) Schematic of the experimental apparatus. Experimental setup for measurement of (b) longitudinal; (c) flexural displacements.
- Fig. 13. Experimental results. (a) Modulus of impedance. (b) Phase.
- Fig. 14. Measured response of the (a) longitudinal; (b) flexural vibration amplitudes of the horn tip.
- Fig. 15. Measured vibration amplitude of the horns as functions of the driving voltage.
- Fig. 16. Harmonic response of the designed and fabricated Bézier horns.

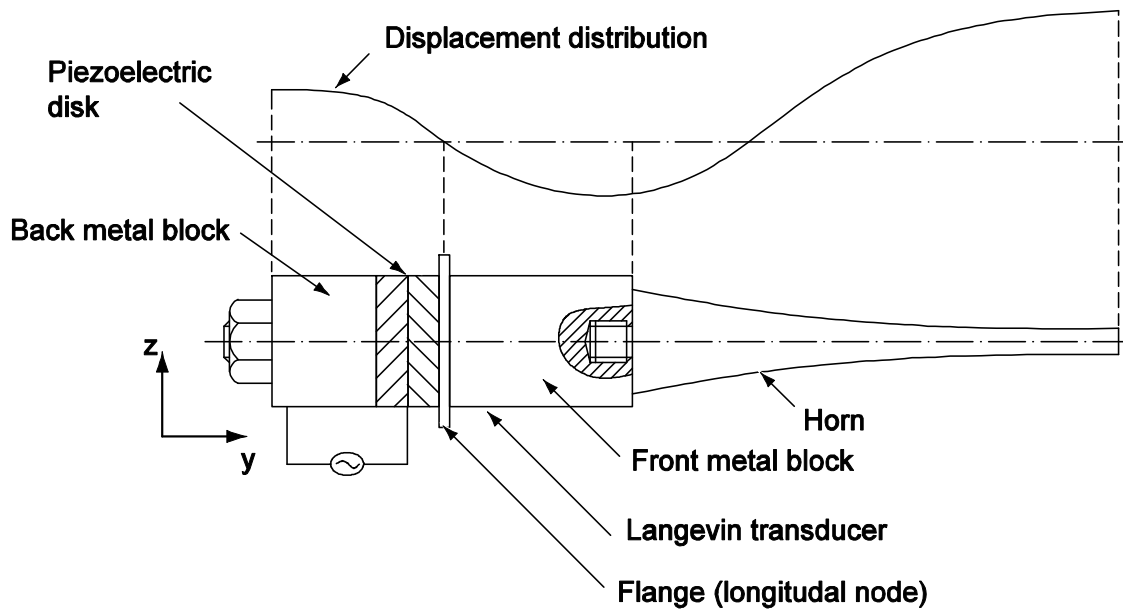


Fig. 1. Schematic of a horn and a Langevin transducer.

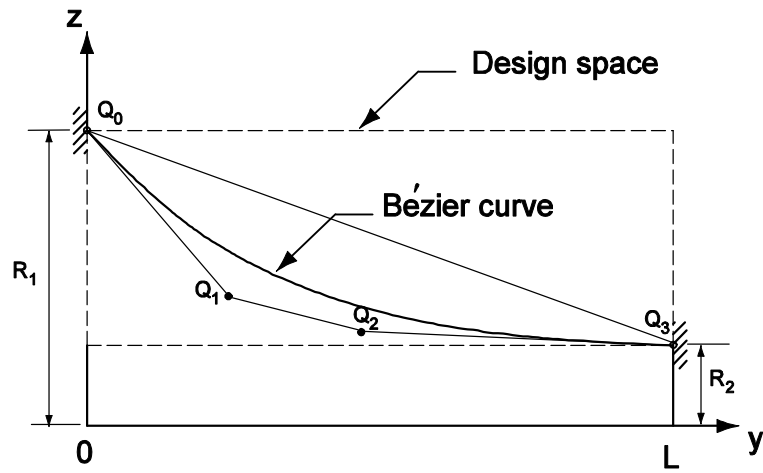


Fig. 2. A profile of a Bézier horn and its four control points  $Q_0$ ,  $Q_1$ ,  $Q_2$  and  $Q_3$ .

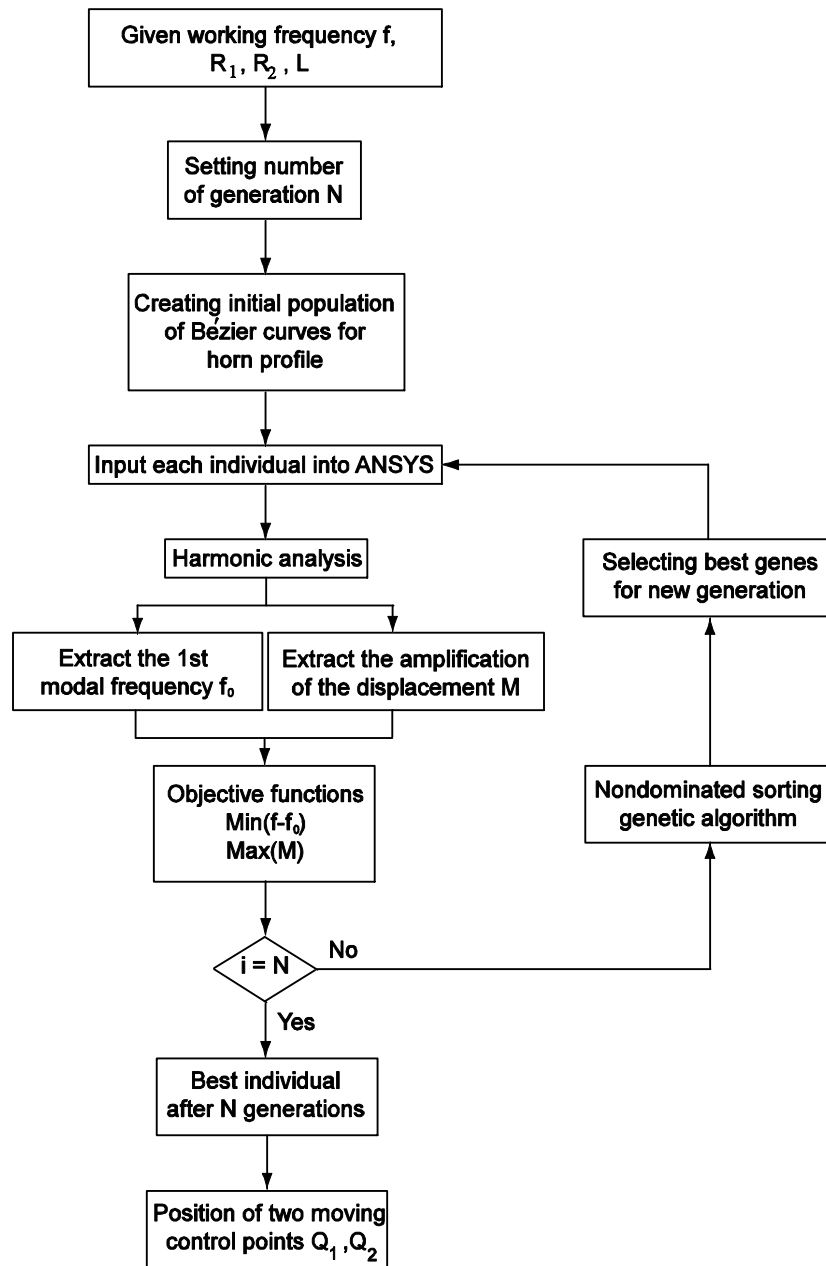


Fig. 3. Flowchart of the optimization procedure.

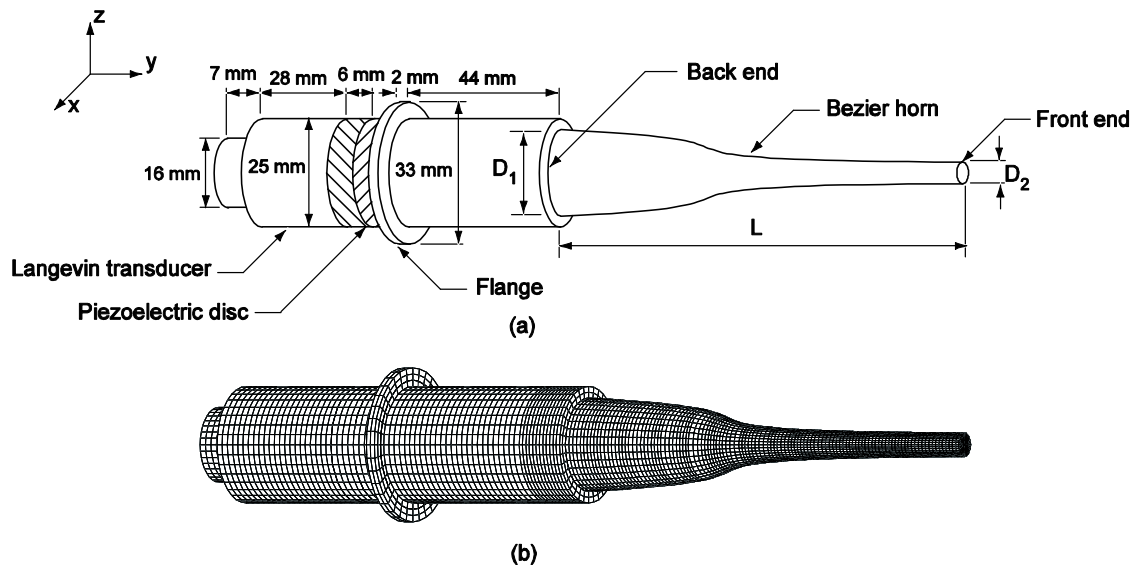


Fig. 4. (a) Schematic of a horn and a Langevin transducer. (b) A mesh for a three-dimensional finite element model.

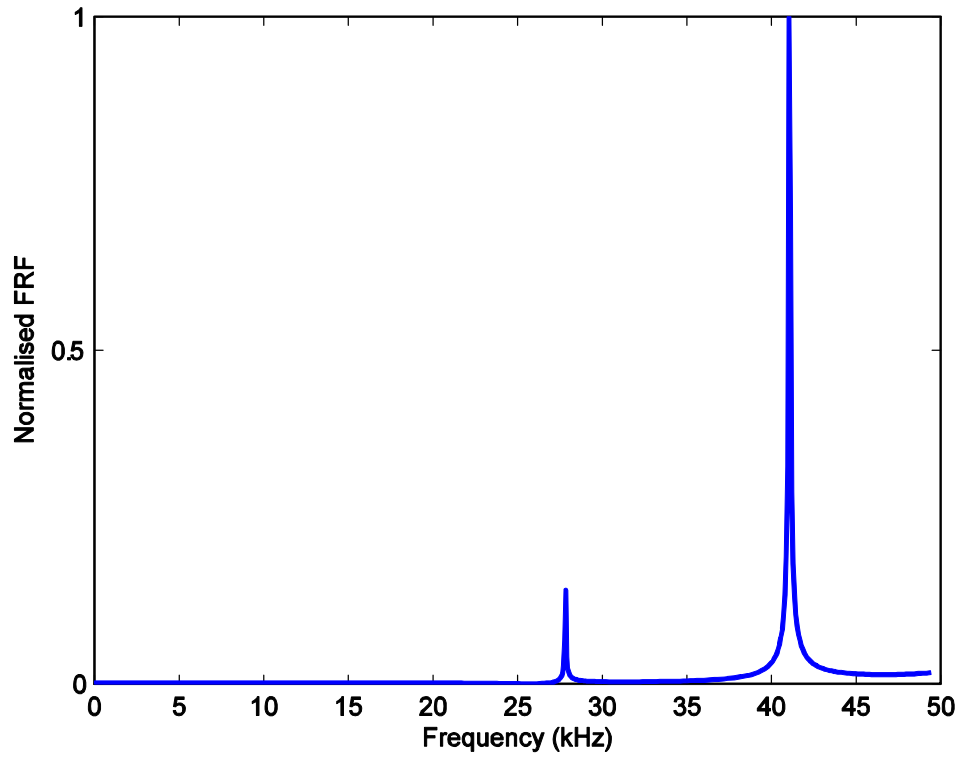


Fig. 5. A typical normalized frequency response function of the model.

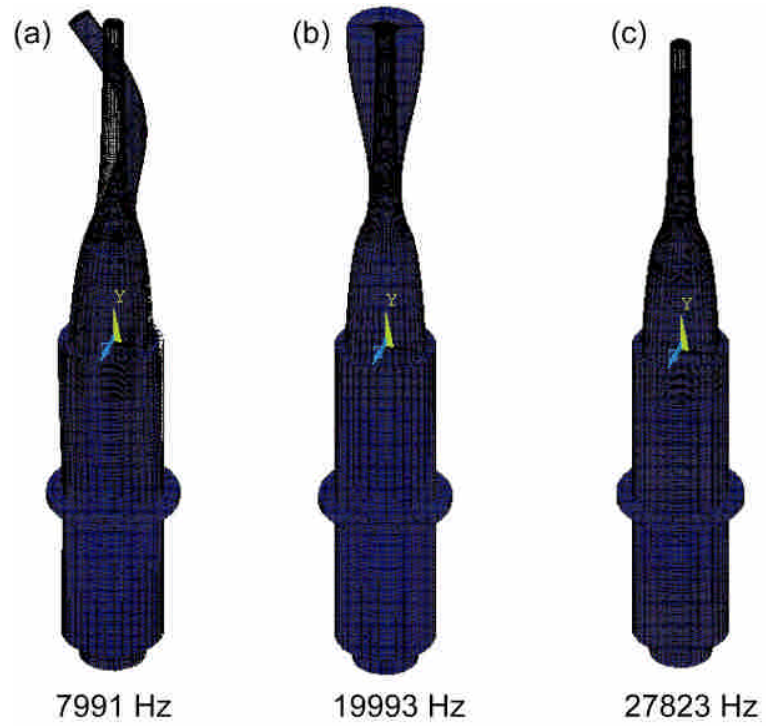


Fig. 6. The internal modes determined by finite element analyses.

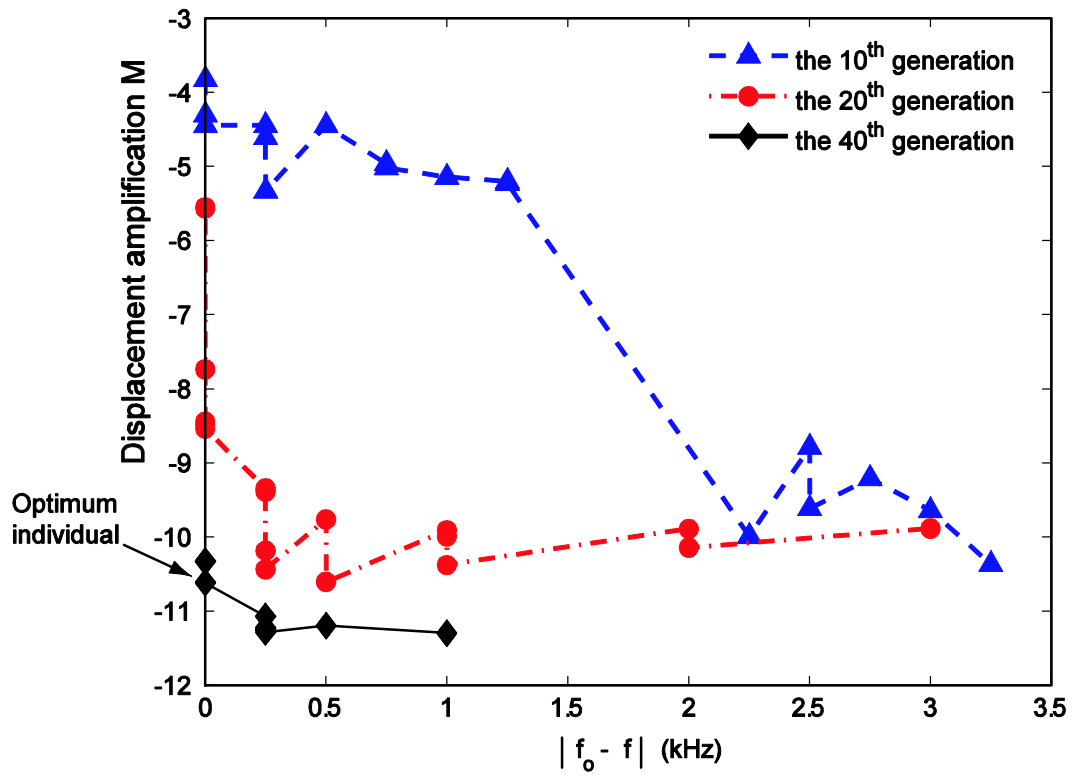


Fig. 7. Distribution of the population of several generations in the optimization process.

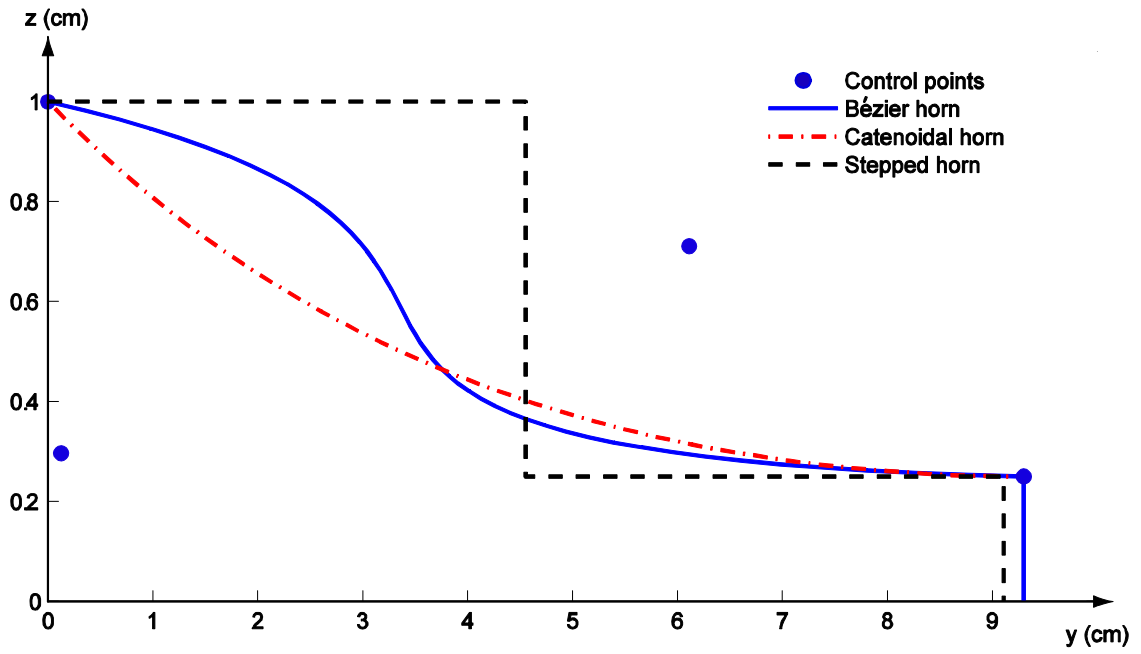


Fig. 8. Profiles of the horns.

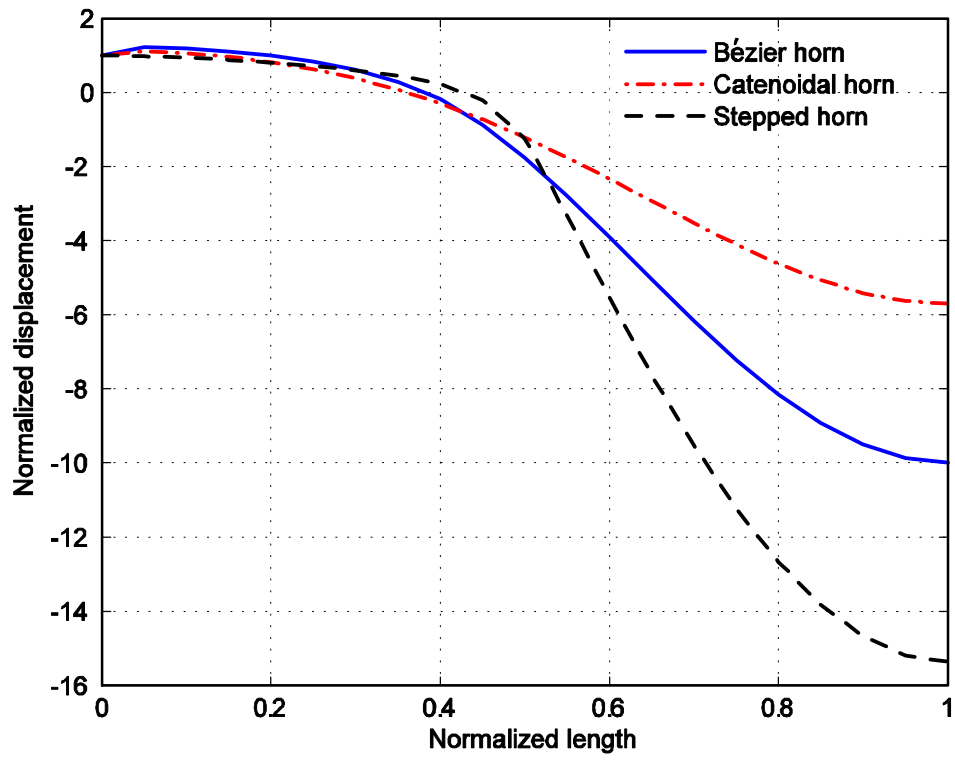


Fig. 9. Normalized displacements along the normalized length of the horns.

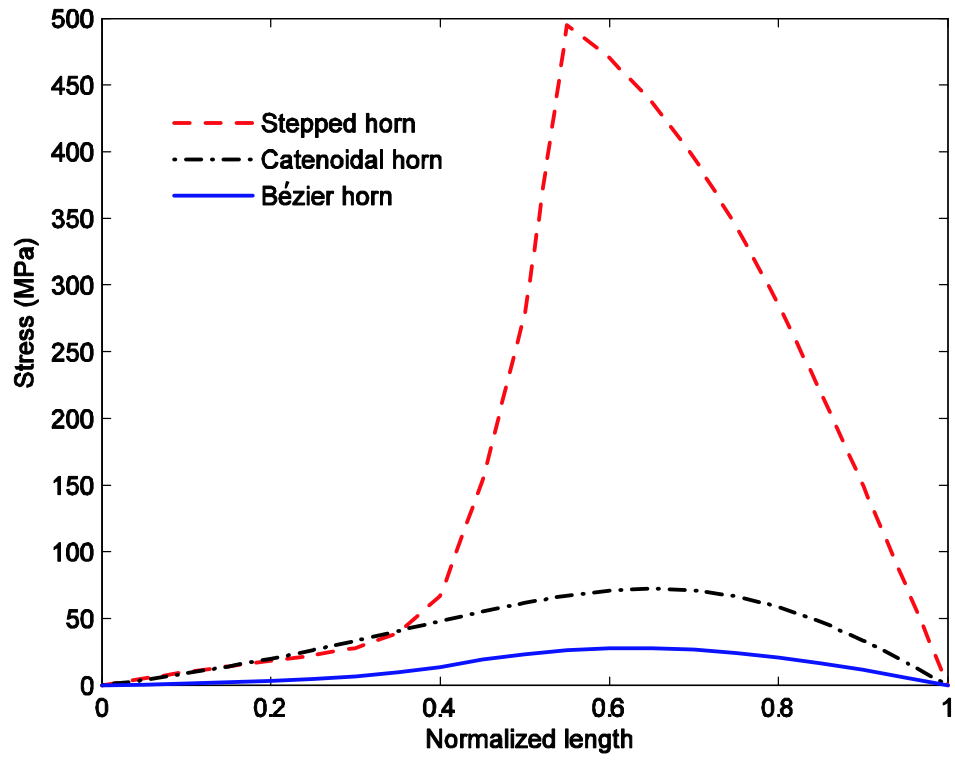


Fig. 10. Von Mises stress along the normalized length of the horns.

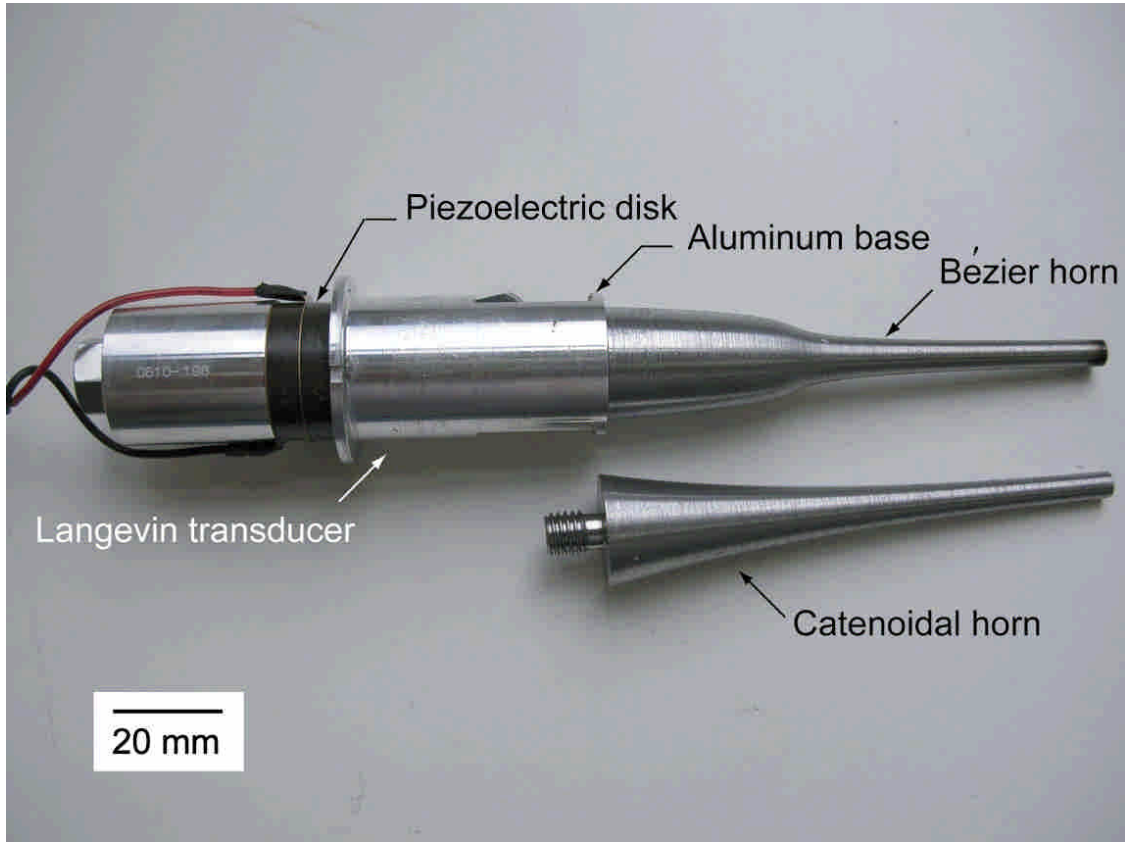
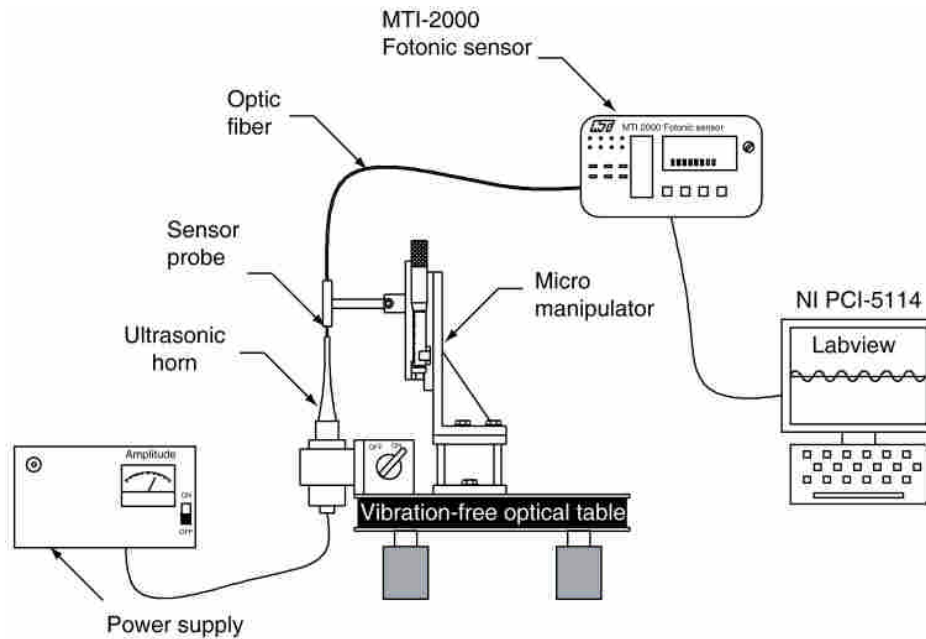
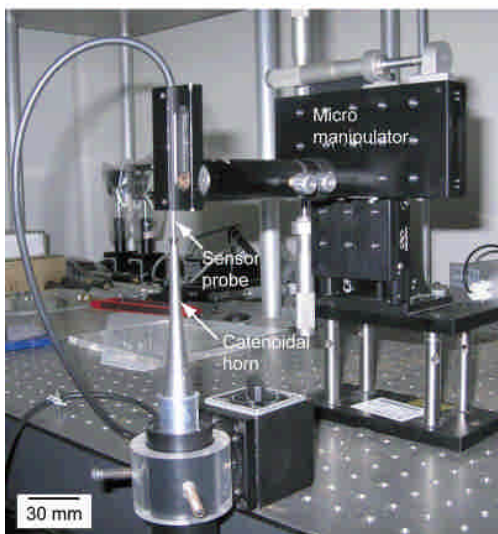


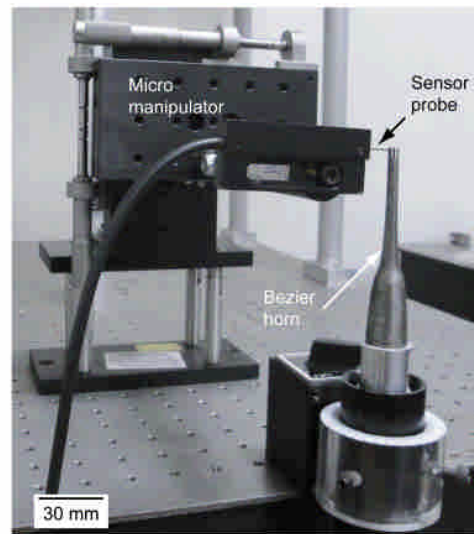
Fig. 11. Fabricated prototypes and a Langevin transducer.



(a)

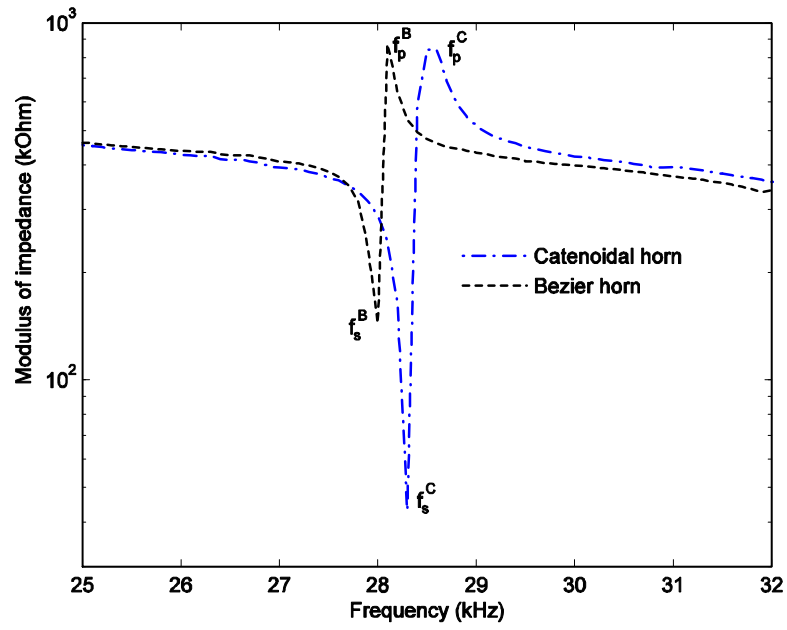


(b)

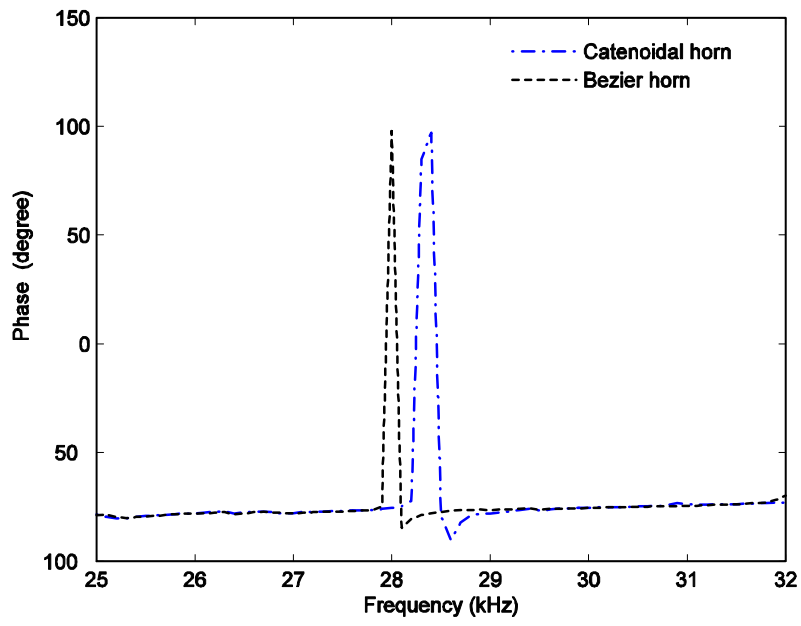


(c)

Fig. 12. (a) Schematic of the experimental apparatus. Experimental setup for measurement of (b) longitudinal; (c) flexural displacements.

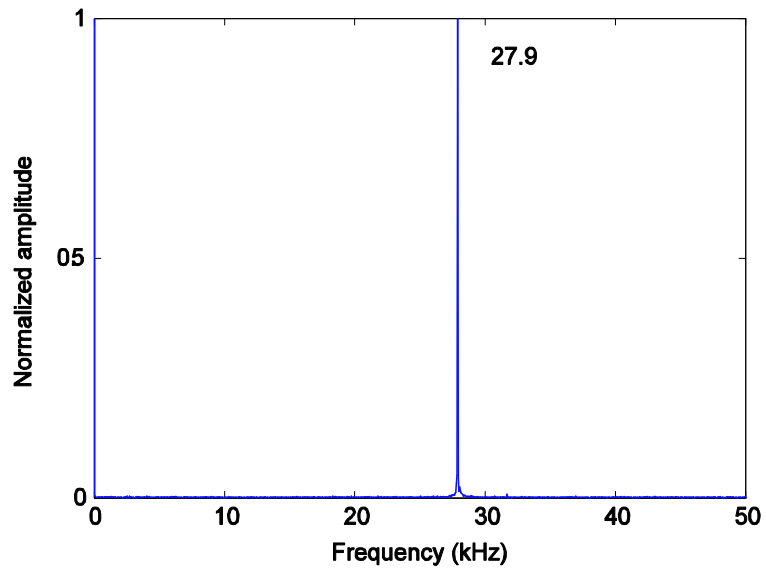


(a)

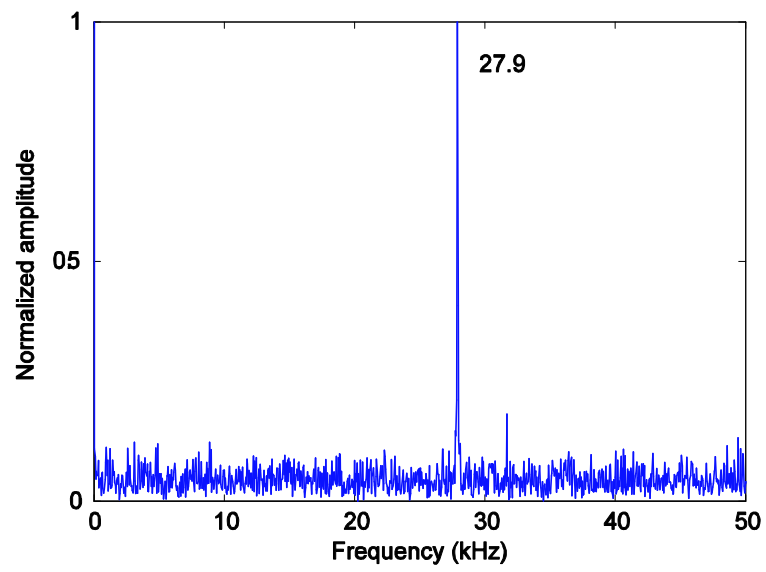


(b)

Fig. 13. Experimental results. (a) Modulus of impedance. (b) Phase.



(a)



(b)

Fig. 14. Measured response of the (a) longitudinal; (b) flexural vibration amplitudes of the horn tip.

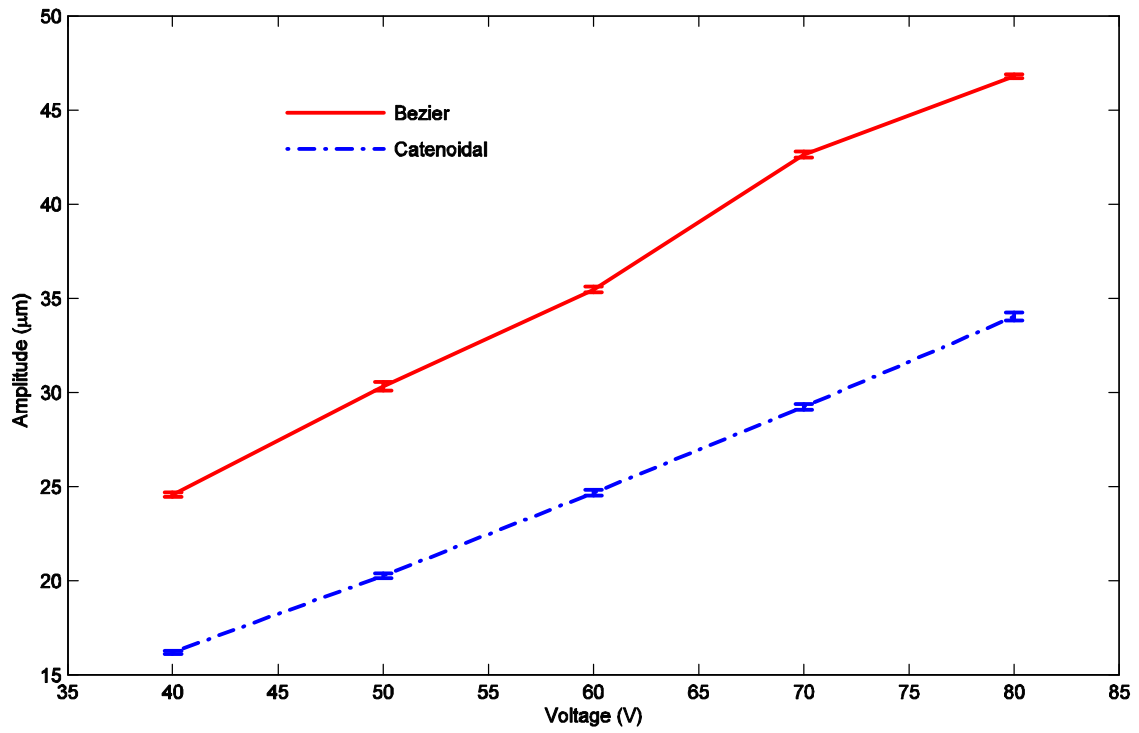


Fig. 15. Measured vibration amplitude of the horns as functions of the driving voltage.

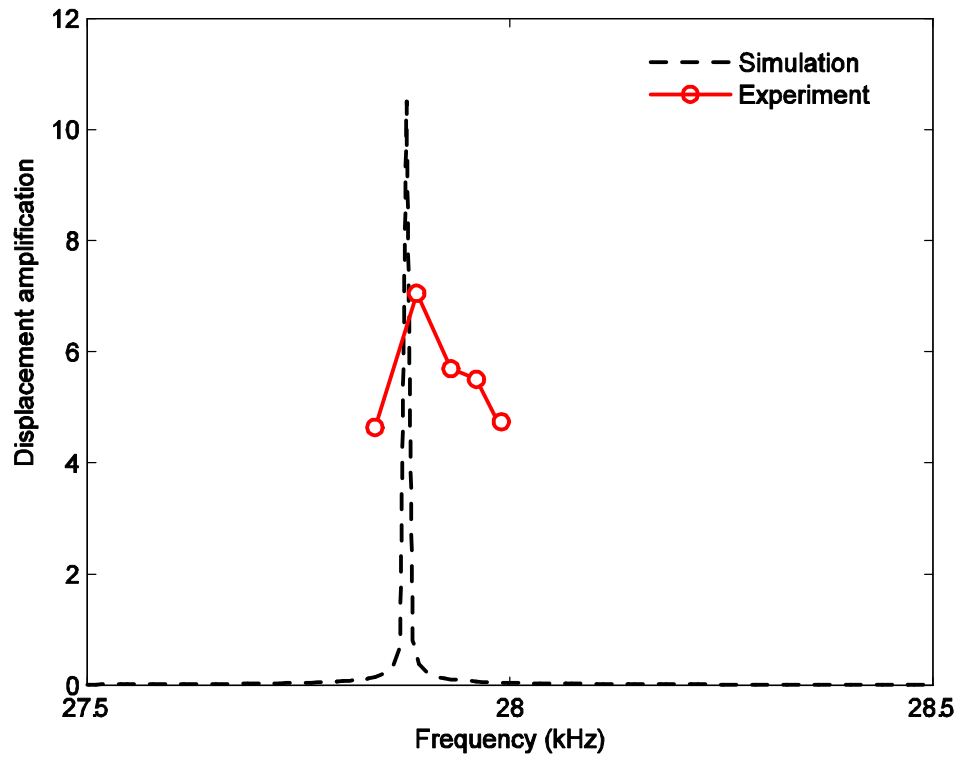


Fig. 16. Harmonic response of the designed and fabricated Béziers horns.